JACS
JOURNAL OF THE AMERICAN CHEMICAL SOCIETY
Article
pubs.acs.org/JACS

A New Rechargeable Sodium Battery Utilizing Reversible Topotactic Oxygen Extraction/Insertion of $CaFeO_z$ ($2.5 \leq z \leq 3$) in an Organic Electrolyte

Mitsuhiro Hibino,*[,†] Ryuji Harimoto,[†] Yoshiyuki Ogasawara,[†] Ryota Kido,[†] Akira Sugahara,[†] Tetsuichi Kudo,[†] Eita Tochigi,[‡] Naoya Shibata,[‡] Yuichi Ikuhara,[‡] and Noritaka Mizuno*[,†]

[†]Department of Applied Chemistry, School of Engineering, The University of Tokyo, 7-3-1 Hongo, Bunkyo-ku, Tokyo 113-8656, Japan

[‡]Institute of Engineering Innovation, School of Engineering, The University of Tokyo, Yayoi 2-11-16, Bunkyo-ku, Tokyo 113-8656, Japan

Supporting Information

ABSTRACT: At present, significant research efforts are being devoted both to identifying means of upgrading existing batteries, including lithium ion types, and also to developing alternate technologies, such as sodium ion, metal−air, and lithium−sulfur batteries. In addition, new battery systems incorporating novel electrode reactions are being identified. One such system utilizes the reaction of electrolyte ions with oxygen atoms reversibly extracted and reinserted topotactically from cathode materials. Batteries based on this system allow the use of various anode materials, such as lithium and sodium, without the requirement to develop new cathode intercalation materials. In the present study, this concept is employed and a new battery based on a $CaFeO_3$ cathode with a sodium anode is demonstrated.

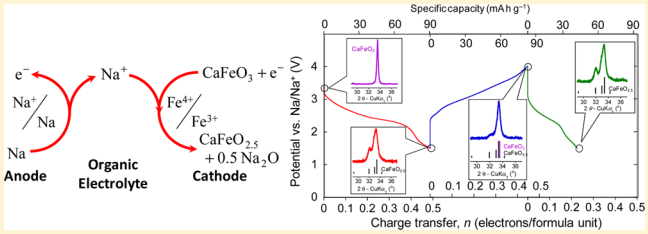

INTRODUCTION

Lithium ion, lithium−air, and lithium−sulfur batteries, all of which operate on different principles, have been widely studied to date.[1−4] In addition, batteries incorporating sodium or magnesium rather than lithium have also been investigated as alternative energy sources.[5−8] In regard to the application of these batteries as power sources for electric vehicles or as components of solar and wind power generation systems, it is evident that additional improvements are necessary in terms of capacity, energy density, and cost.

We have recently both proposed and demonstrated an oxygen rocking battery in which oxygen atoms are shuttled between a cathode and an anode composed of iron-based perovskite oxides $Ca_{0.5}La_{0.5}FeO_z$, with $2.58 \leq z \leq 2.63$ for the anode and $2.75 \leq z \leq 2.863$ for the cathode. These materials have been found to allow topotactic and reversible extraction/insertion of oxygen atoms.[9] During the course of this research, we developed the concept of a battery based on a combination of a perovskite-type cathode and a low-electrode-potential anode that can achieve high energy densities through the use of organic rather than aqueous electrolytes.

The present report describes a battery of this type (see Figure 1) consisting of a $CaFeO_3$ cathode and a sodium anode, both of which are inexpensive and nontoxic materials, in conjunction with a $NaClO_4$/triglyme electrolyte and evaluates this battery system from a basic viewpoint. During discharge, the $CaFeO_3$ cathode undergoes topotactic extraction of oxygen atoms and changes to $CaFeO_{2.5}$, and the extracted oxygen atoms react with sodium ions to form sodium oxides. This cathode has a theoretical specific capacity of 187 mA h g^{-1} if the final discharge product is Na_2O.

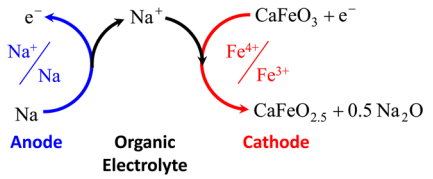

Figure 1. A new rechargeable sodium battery utilizing reversible topotactic oxygen extraction/insertion in iron-based $CaFeO_z$ ($2.5 \leq z \leq 3$) in an organic electrolyte.

RESULTS AND DISCUSSION

Synthesis and Characterization of $CaFeO_3$. $CaFeO_3$, in which all of the iron ions are in the tetravalent state, has been synthesized by oxidation of $CaFeO_{2.5}$ at high oxygen pressures and high temperatures (typically several GPa and 750−1100 °C).[10,11] We have, however, developed an alternative process that allows the oxidation of $CaFeO_{2.5}$ under milder conditions. This process consists of a reaction with sodium hypochlorite in an aqueous solution at 80 °C and is based on a similar method

Received: November 12, 2013
Published: December 17, 2013

   dx.doi.org/10.1021/ja411365z | J. Am. Chem. Soc. 2014, 136, 488−494

that has been applied to the synthesis of $La_2CuO_{4+\delta}$.[12] Figure 2 presents the X-ray diffraction (XRD) profile and Mössbauer

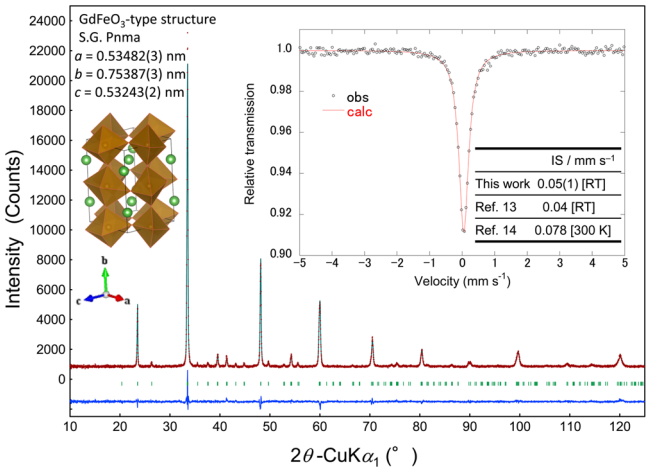

Figure 2. Observed and calculated XRD profiles and (inset) the Mössbauer spectrum of $CaFeO_3$. The calculated XRD profile was determined via Rietveld analysis.

spectrum of a $CaFeO_3$ sample thus synthesized. All of the XRD peaks were indexed to the $GdFeO_3$-type (orthorhombic perovskite-type) structure, to which $CaFeO_3$ is isomorphic.[10] A Rietveld analysis was successfully performed and resulted in a goodness-of-fit value of 1.275 on the basis of the $GdFeO_3$-type structure [space group *Pnma*, a = 0.53482(3) nm, b = 0.75387(3) nm, c = 0.53243(2) nm]. The refined atomic positions and displacement parameters along with the associated R values are summarized in Table S1 in the Supporting Information. The Mössbauer spectrum was well fit using a single paramagnetic component with an isomer shift of 0.05 mm s^{-1}, assignable to Fe^{4+}.[13,14] Taken together, these results indicate that the synthesized material was identified with a high degree of certainty as pure $CaFeO_3$, demonstrating that we were successful in preparing $CaFeO_3$ from $CaFeO_{2.5}$ under mild conditions.

Electrode Properties. Figure 3 shows the potential profile of $CaFeO_3$ during electrochemical reduction (discharge) and reoxidation (charge) processes at a current density of 3.72 mA

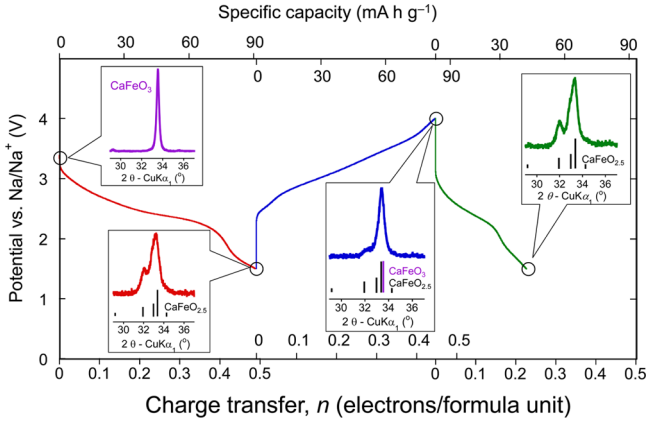

Figure 3. Discharge and charge profiles of $CaFeO_3$ in constant-current mode. The ex situ XRD patterns of the electrodes in the main peak region are also shown. The pattern for $CaFeO_{2.5}$ (JCPDS no. 47-1744) is also shown by the solid lines.

g^{-1}. During reduction to 1.5 V and reoxidation to 4.0 V, the material exhibits charge transfers of 0.49 (corresponding to 91 mA h g^{-1}), 0.45 (84 mA h g^{-1}), and 0.23 (43 mA h g^{-1}) for the first reduction, the first oxidation, and the second reduction, respectively. Ex situ XRD patterns of the electrodes within the main peak regions are also provided in Figure 3 (for profiles over a wider range of angles, see Figure S1 in the Supporting Information). Reduction resulted in the appearance of peaks attributable to a brownmillerite-type phase (BM-phase) with significantly smaller peaks associated with the perovskite-type phase (P-phase).[15] After the first reduction, the P-phase and BM-phase mole fractions were estimated from the Rietveld analysis to be 0.07(9) and 0.93(9), respectively, from which the average valence of the iron ions was estimated to be 3.07(9) on the assumption of $CaFe^{4+}O_3$ and $CaFe^{3+}O_{2.5}$ for the P- and BM-phases, respectively. The change in the average valence of iron ions from 4.00 to 3.07(9) corresponds to a charge transfer of n = 0.465(5) upon the formation of Na_2O_2 (Figure S3B in the Supporting Information). The charge transfer in the first reduction was 0.486, a little larger than 0.465. The difference is probably responsible for the formation of a solid−electrolyte interphase (SEI). Following reoxidation, the P-phase peaks reappeared, and at this point the P-phase and BM-phase mole fractions were 0.75(2) and 0.25(2), respectively. These results demonstrate that the electrochemical reduction and reoxidation reactions in the organic electrolyte progress via transitions between the P-phase and the BM-phase through the extraction and reinsertion of oxygen atoms. The incomplete recovery from the BM-phase to the P-phase during the oxidation process could be explained by oxidative decomposition of the electrolyte solvent and/or sodium oxides to evolve oxygen. Further reduction of the reoxidized sample again resulted in the formation of a BM-phase. The P-phase and BM-phase mole fractions were 0.05(1) and 0.95(1), respectively. The specific capacity decreased from the first reduction to the second one. This is probably because of the decrease in the mole fraction of the P-phase from the first reduction to the second one, the formation of the SEI, and the disorder of the electrode material suggested by the XRD line broadening.

It has been reported that $CaFeO_{2.5}$ does not undergo electrochemical oxidation in an aqueous electrolyte solution, while the oxidation of $Ca_{1-x}Sr_xFeO_{2.5}$ is possible only for x > 0.25.[16] It is probable that we were able to successfully oxidize the calcium iron oxide BM-phase in our work because our use of an organic electrolyte with a wide potential window allowed us to apply a high overpotential to the electrode. The chemical potential of oxygen in the P-phase and BM-phases of $CaFeO_z$ upon the coexistence of the two phases versus $^1/_2O_2$ (gaseous oxygen) under standard conditions (298 K, 10^5 Pa), was estimated to be $\mu_{O,P\text{-}BM}$ = 19.5 kJ mol^{-1} from the open-circuit potentials as described later, indicating that the electrochemical oxidation from the BM-phase to the P-phase requires a potential that is 0.101 V ($=\mu_{O,P\text{-}BM}/2F$) greater than the equilibrium potential for oxygen evolution [$O_2 + 2H_2O + 4e^- \rightarrow 4OH^-$: $\phi = (1.23 - 0.0591 \times pH)$ V vs SHE]. This suggests that oxidation in aqueous electrolyte solutions is difficult because of the evolution of oxygen.

We also synthesized the iron-based perovskite-type $SrFeO_3$ phase using the same method as applied for the synthesis of $CaFeO_3$, and we found that the material could be reversibly reduced and reoxidized in an organic electrolyte using not only a sodium anode [46 mA h g^{-1} (0.02 C)] but also a lithium anode [63 mA h g^{-1} (0.04 C); $CaFeO_3$: 78 mA h g^{-1} (0.2 C)]

dx.doi.org/10.1021/ja411365z | J. Am. Chem. Soc. 2014, 136, 488−494

and a magnesium anode [42 mA h g^{-1} (0.01 C)], showing the wide applicability of the present battery system.

$CaFeO_z$ Structural Changes. Figure 4A shows the ex situ XRD patterns of $CaFeO_z$ samples at various reduction levels.

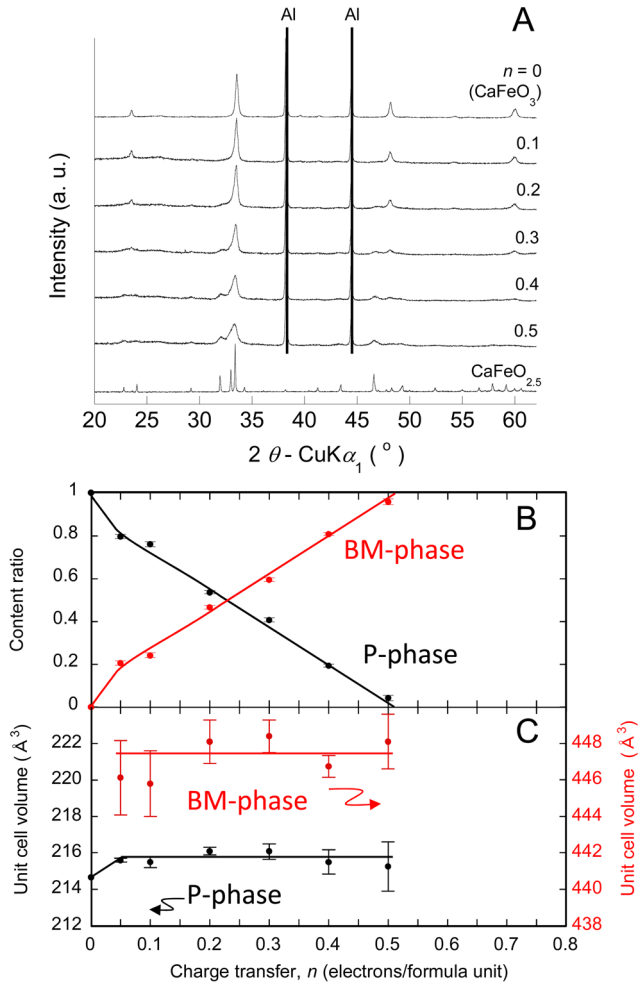

Figure 4. (A) Changes in XRD profiles of $CaFeO_z$ with n, and (B) molar fractions and (C) unit cell volumes of the P- and BM-phases calculated from the Rietveld analysis.

All of the diffraction peaks could be indexed to the P- and BM-phases by Rietveld analysis. The mole fractions of the P-phase and the BM-phase as functions of charge transfer (n) are summarized in Figure 4B. The BM-phase was observed in addition to the P-phase at n = 0.05, and the BM-phase content increased over the range of n from 0.05 to 0.5[17] while the unit cell volumes of the P- and BM-phases were unchanged (Figure 4C). The slight increase in the unit cell volume of the P-phase from 214.67(2) to 215.6(5) Å^3 within the range of $0 \leq n \leq 0.05$ would result from the formation of oxygen vacancies in increasing amounts with the progress of the reduction. The unit cell volume of the BM-phase in the two-phase region of $0.05 \leq n \leq 0.5$ [447.5(30) Å^3] is close to that of $CaFeO_{2.521(3)}$ [449.18(3) Å^3], the material used as the precursor in the synthesis of $CaFeO_3$, which suggests that the composition of the BM-phase in the range of $0.05 \leq n \leq 0.5$ is $CaFeO_{2.52}$.

Observation and Analysis of the Electrode Reduced to n = 0.5. Figure 5 shows a scanning transmission electron microscopy (STEM) image and the corresponding energy dispersive X-ray spectroscopy (EDS) maps of the Ca, Fe, and

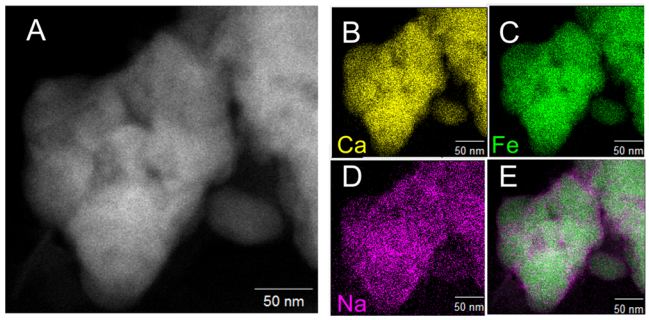

Figure 5. (A) STEM image of the electrode sample reduced to n = 0.5. (B–D) Elemental maps obtained by EDS analysis. (E) Superposition of the Fe and Na maps.

Na distributions of the sample reduced to n = 0.5. Ca and Fe were uniformly distributed over the surface of the particle, and the images overlapped each other. The Ca/Fe ratio was 1/1 (Table S2 and Figure S2 in the Supporting Information). In contrast, the superposition of the Fe and Na distributions (Figure 5E) showed that Na also existed outside the Fe-distributed region, suggesting the presence of Na-containing compounds on the surface of the particle.[18] The Na/Fe ratio was 0.25(5) (Table S2 and Figure S2 in the Supporting Information), which is smaller than the value of 0.5 estimated with n = 0.5. The smaller value of 0.25 is possibly explained by detachment of Na-containing compounds from the particle surface during preparation of the sample for the STEM-EDS analyses (i.e., washing of the electrode to remove the electrolyte).

The electron diffraction (ED) pattern of the sample reduced to n = 0.5 is displayed in Figure 6. The most intense spots were

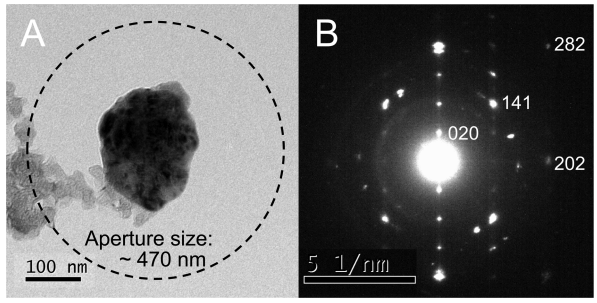

Figure 6. (A) Particles of the electrode sample reduced to n = 0.5 for ED measurement and size of the selected-area aperture. The small, low-contrast particles are carbon ones added as a conducting material. (B) ED pattern of the particles.

assigned to $CaFeO_{2.5}$ with the electron beam incident along $\langle 10\bar{1} \rangle$. All of the other spots were attributable to $CaFeO_{2.5}$ oriented in other directions. The halo rings were due to the carbon added as the conducting material. No spots due to crystalline Na-containing compounds were observed, suggesting that the Na-containing compounds were amorphous and/or nanocrystalline.

Direct observation of the Na-containing compounds for the sample reduced to n = 0.5 was attempted with high-resolution transmission electron microscopy (HRTEM). Figure 7A shows the image near the surface of the particle (150–200 nm in size). The fringe region with a period of 0.74 nm was assigned to the {020} plane of $CaFeO_{2.5}$ (Figure 7B). On the outer surface of the particle, multiple fringe regions with a period of 0.34 nm

dx.doi.org/10.1021/ja411365z | J. Am. Chem. Soc. 2014, 136, 488–494

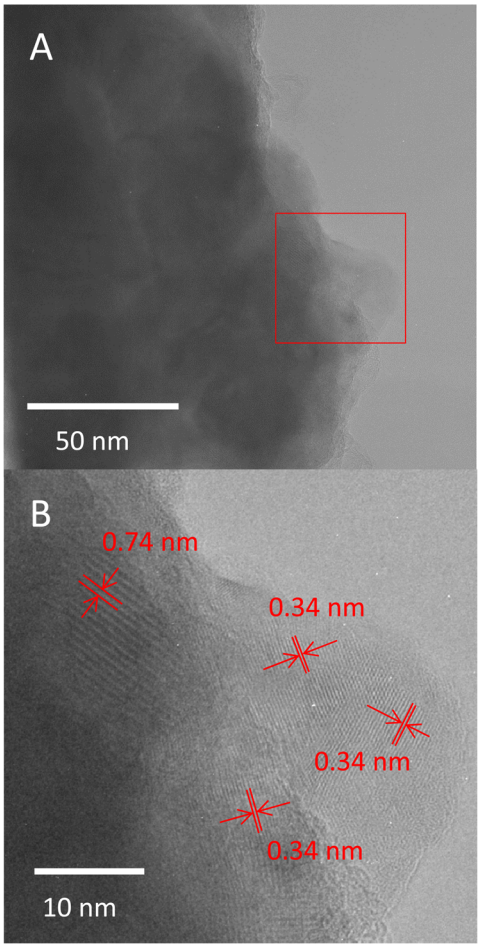

Figure 7. (A) HRTEM image of the sample reduced to n = 0.5. (B) Magnified image of the red rectangular area in (A).

were observed in areas with sizes of 10−20 nm. The observed period (0.34 nm) is approximately equal to those of the {121} plane of $CaFeO_{2.5}$ (0.345 nm)[19] and the {101} plane of Na_2O_2 (0.344 nm).[20] The image contrast of $CaFeO_{2.5}$ easily exhibits a lattice pattern formed by multiple diffracted beams because of its large unit cell (a = 0.5595 nm, b = 1.483 nm, c = 0.5431 nm),[19] even when the incident electron beam did not coincide with the zone axis in the crystal. In fact, we could not obtain the fringe of the {121} plane of $CaFeO_{2.5}$ with the simulation by changing the observation direction. In contrast, Na_2O_2 with a smaller unit cell (a = 0.6208, c = 0.4469)[20] allows a wide range of observation directions in which only the fringe of the {101} plane is formed (see section 4 in the Supporting Information). Therefore, a plurality of the fringe regions with a period of 0.34 nm are likely due to Na_2O_2.

Thermodynamic Estimation of Electrode Potentials. The chemical potential of oxygen atoms in $CaFeO_z$ ($2.5 \le z \le 3$) versus $^1/_2O_2$ (gaseous oxygen) under standard conditions (298 K, 10^5 Pa) is expressed by $\mu_O(z)$, and a plot showing changes in $\mu_O(z)$ with oxygen content is shown in Figure 8A. On the basis of the standard Gibbs free energies of formation of NaO_2, Na_2O_2, and Na_2O,[21] $-\Delta G_f(NaO_2)/F$, $-\Delta G_f(Na_2O_2)/2F$, and $-\Delta G_f(Na_2O_2)/2F$ were calculated to be 2.267, 2.330, and 1.964 V versus Na/Na^+, respectively. Therefore, the electrode potentials at which oxygen atoms in $CaFeO_z$ are given by the following eqs 1, 2 and 3.

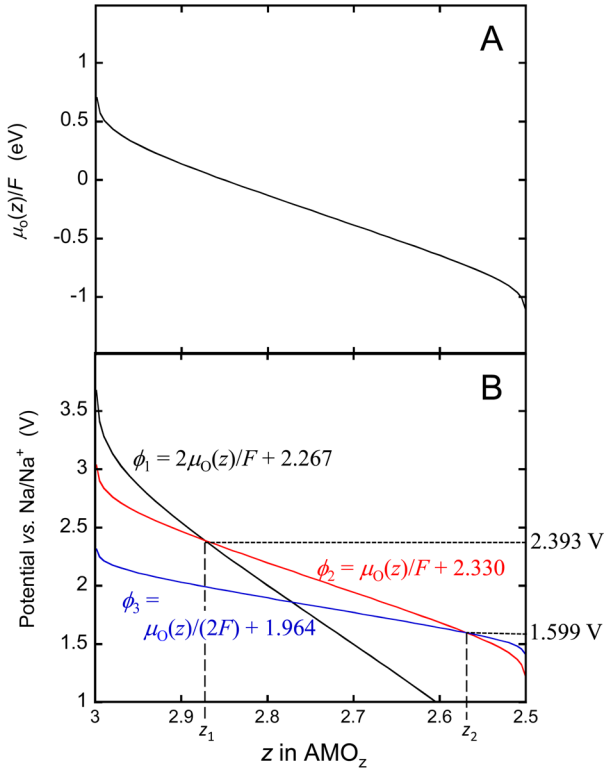

Figure 8. Plots of (A) the chemical potential of oxygen, $\mu_O(z)$, and (B) the electrode potentials ϕ_1, ϕ_2, and ϕ_3 as functions of oxygen content z in a metal oxide (AMO_z).

$$O(\text{in } CaFeO_z) + \frac{1}{2}Na^+ + \frac{1}{2}e^- \rightarrow \frac{1}{2}NaO_2:\ \phi_1 = \frac{2\mu_O(z)}{F} + 2.267\ \text{V} \quad (1)$$

$$O(\text{in } CaFeO_z) + Na^+ + e^- \rightarrow \frac{1}{2}Na_2O_2:\ \phi_2 = \frac{\mu_O(z)}{F} + 2.330\ \text{V} \quad (2)$$

$$O(\text{in } CaFeO_z) + 2Na^+ + 2e^- \rightarrow Na_2O:\ \phi_3 = \frac{\mu_O(z)}{2F} + 1.964\ \text{V} \quad (3)$$

Figure 8B shows ϕ_1, ϕ_2, and ϕ_3 as functions of z. The intersection of ϕ_1 and ϕ_2 ($z = z_1$) shows the potential associated with the coexistence of NaO_2 and Na_2O_2, while that of ϕ_2 and ϕ_3 ($z = z_2$) shows the potential associated with the coexistence of Na_2O_2 and Na_2O. The potentials of those intersections are identical to the potentials shown in eqs 4 and 6, respectively.

$$NaO_2 + Na^+ + e^- \rightarrow Na_2O_2:\ \phi_{NaO_2-Na_2O_2} = 2.393\ \text{V},\ \frac{\mu_O(z)}{F} = 0.063\ \text{eV} \quad (4)$$

$$NaO_2 + 3Na^+ + 3e^- \rightarrow 2Na_2O:\ \phi_{NaO_2-Na_2O} = 1.864\ \text{V},\ \frac{\mu_O(z)}{F} = -0.20\ \text{eV} \quad (5)$$

dx.doi.org/10.1021/ja411365z | J. Am. Chem. Soc. 2014, 136, 488−494

$$Na_2O_2 + 2Na^+ + 2e^- \rightarrow 2Na_2O:\ \phi_{Na_2O_2-Na_2O} = 1.599\ V,\quad \frac{\mu_O(z)}{F} = -0.73\ eV \tag{6}$$

Thermodynamically, electrochemical reduction should proceed in the order of (1) → (4) → (2) → (6) → (3). Therefore, the change transfer versus potential can be estimated as follows:

I. $0 \le n \le (3 - z_1)/2$: NaO_2 is formed by the reaction of O (in $CaFeO_z$) with Na^+ (in the electrolyte).
II. $(3 - z_1)/2 \le n \le (3 - z_1)$; Na_2O_2 is formed from the NaO_2 generated in step I.
III. $(3 - z_1) \le n \le (3 - z_2)$; Na_2O_2 is formed from O (in $CaFeO_z$) and Na^+ (in the electrolyte).
IV. $(3 - z_2) \le n \le 2(3 - z_2)$; Na_2O is formed from the Na_2O_2 generated in steps II and III.
V. $2(3 - z_2) \le n \le 1$; Na_2O is formed from O (in $CaFeO_z$) and Na^+ (in the electrolyte).

Figure 9A displays the potentials thermodynamically estimated as a function of n. If z_2 is fairly close to 2.5, the range of step V is too narrow to be observed. As shown in Figure 4, the electrochemical reduction of $CaFeO_3$ proceeds during the coexistence of the P- and BM-phases. In general, the potential of the two-phase reaction is constant. Figure 9B shows the thermodynamically estimated potential profile when z_1 is close to 2.5, at which point the potential associated with the coexistence of the P- and BM-phases is slightly higher than 2.393 V and closely matches the experimental data plotted in Figure 10 (see below).

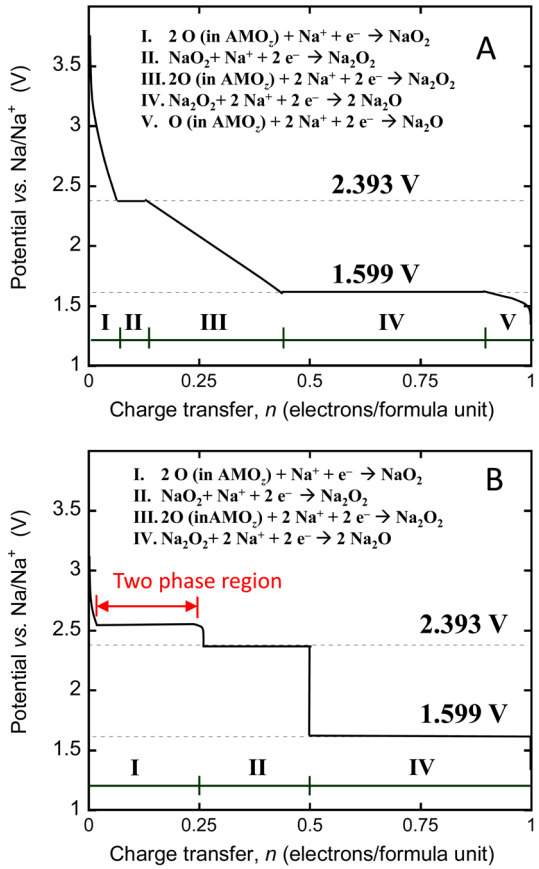

Figure 9. (A) Potentials of the metal oxide (AMO_z) thermodynamically estimated as a function of n. (B) Potentials when z_1 is close to 2.5 and the potential in the coexistence of two phases is slightly higher than 2.393 V.

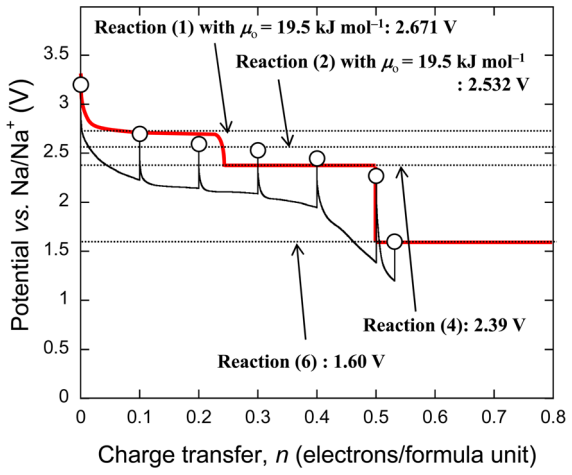

Figure 10. Open-circuit potentials (open circles), GITT curve (black line), and thermodynamically estimated path (red line).

Open-Circuit Potentials (OCPs) and Reaction Mechanisms. OCPs were obtained using the galvanostatic intermittent titration technique (GITT) during the electrochemical reduction and are shown in Figure 10. The potentials initially decreased as n increased from 0.0 to 0.1 and then plateaued at around 2.52 V for n = 0.1 to 0.4. As noted earlier, the P- and BM-phases coexist over the range of $0.05 \le n \le 0.5$ (Figure 4B). This plateau region must correspond to reaction 1, which produces NaO_2 using the oxygen atoms in $CaFeO_3$, since the measured potential of 2.52 V is greater than the potential of 2.393 V associated with reaction 4. The value of μ_O for the P- and BM-phases in their two-phase region can be estimated as approximately 19.5 kJ mol^{-1} from eq 1. Thermodynamically, the potential is expected to remain constant at 2.52 V with increasing n until only the BM-phase ($CaFeO_{2.52}$) is present. Since the reduction of $CaFeO_{2.52}$ to $CaFeO_{2.50}$ requires only a minimal amount of charge transfer, it should readily proceed in the single BM-phase at approximately n = 0.25. Subsequent to this, reaction 4 proceeds from n = 0.25 to 0.5 at 2.393 V, followed by the reduction of Na_2O_2 to Na_2O from n = 0.5 to 1.0 according to reaction 6. At n = 0.5, only $CaFeO_{2.5}$ and Na_2O_2 are estimated to be present, which is supported by the observation of $CaFeO_{2.5}$ and Na_2O_2 by HRTEM. The red line in Figure 10 tracks the thermodynamically estimated potentials. The observed potentials are approximately equivalent to the values described by the red line within the range of $0 \le n \le 0.5$. The deviation is explained by the initiation of the thermodynamically unfavorable reaction 2, which occurs simultaneously with reactions 1 ($0.1 \le n \le 0.2$) and 4 ($0.3 \le n \le 0.5$) as a result of high overpotentials, as indicated by the GITT curve. As a result, before the equilibrium state is reached, the potential at n = 0.2 lies between those of reactions 1 and 2 and the potentials at n = 0.3 and 0.4 lie between those of reactons 2 and 4.

CONCLUSIONS

A new battery consisting of a $CaFeO_3$ cathode with a sodium anode (both of which are inexpensive and nontoxic materials)

dx.doi.org/10.1021/ja411365z | J. Am. Chem. Soc. 2014, 136, 488−494

in conjunction with a $NaClO_4$/triglyme electrolyte has been developed, and its operation has been confirmed. This battery utilizes the reversible electrochemical reduction and reoxidation transition between $CaFeO_3$ and $CaFeO_{2.5}$ through topotactic extraction/reinsertion of oxygen atoms and the formation/decomposition of Na_2O_2. It was also possible to prepare the iron-based perovskite-type material $SrFeO_3$ according to the same method as used to synthesize $CaFeO_3$, and these materials could be reversibly reduced and reoxidized in an organic electrolyte using not only a sodium anode but also lithium and magnesium anodes.

EXPERIMENTAL SECTION

Synthesis of $CaFeO_3$. $CaFeO_{2.5}$ was prepared by solid-state reaction using the following procedure. $CaCO_3$ (>99.99%, 4.00 g) and α-Fe_2O_3 (99.9%, 3.19 g) were mixed together and ground in an agate mortar for 5 h, following which the mixture was heated to 1000 °C at 20 °C min^{-1}, held at 1000 °C for 5 h, and then cooled to room temperature in air. The resulting powder was ground again with an agate mortar and pressed into a thin disk, which was subsequently heated to 1100 °C at 20 °C min^{-1}, held at 1100 °C for 24 h, and cooled to room temperature in air to obtain $CaFeO_{2.5}$. A portion of the $CaFeO_{2.5}$ powder (30 mg) was placed in a polytetrafluoroethylene (PTFE) test tube, and an aqueous solution of sodium hypochlorite (2.83 mol L^{-1}, 5 mL) was added. The mixture was allowed to react with agitation at 80 °C for 4 h. Suspended solids were filtered off, and the product was washed first with 0.01 mol L^{-1} hydrochloric acid and then with distilled water and finally dried under vacuum.

Characterization of Materials. The oxygen contents of samples were determined by iodometric titration. Crystal structures were analyzed by XRD using monochromatized Cu Kα_1 radiation on a RIGAKU Smart-Lab system. In preparation for XRD analysis, an electrochemically reduced sample was removed from its electrochemical cell, mounted in an airtight sample holder under inert gas, and interfaced with the diffractometry system. The states of iron ions were determined by Mössbauer spectroscopy using ^{57}Co at room temperature. The isomer shift (IS) relative to α-Fe and quadrupole splitting (QS) were refined by profile fitting.

Electrochemistry. Electrochemical measurements were performed using a three-electrode beaker cell employing metallic sodium as the counter and reference electrodes and a 1 M $NaClO_4$/triglyme electrolyte solution. A $CaFeO_3$ powder pulverized with a planetary ball mill (Fritsh PL-7), a conducting additive (acetylene black), and a binder (PTFE powder) were mixed in the ratio 79/20/1 (w/w) and ground. The mixture was then pressed on an Al mesh (100 mesh) current collector to form the working electrode. Galvanostatic discharge and charge tests between 1.5 and 4.0 V vs Na/Na^+ at 3.72 mA g^{-1} (= 0.02 C) were performed using three different cells; the first trial measured discharge response, the second discharge and charge, and the third discharge, charge, and redischarge. The C rate is often used to describe battery discharging/charging, and in this study, 1 C was defined as the current density at which one electron per formula unit is transferred in 1 h. Each galvanostatic test was followed by XRD measurements. For the sample reduced to n = 0.5 with constant current 0.02 C, STEM-EDS measurements with an ARM-200F microscope (JEOL, Japan) and a Dry SD100GV detector (JEOL, Japan), ED measurements with a JEM-2010HC microscope (JEOL, Japan), and HRTEM measurements on a JEM-4010 microscope (JEOL, Japan) at an accelerating voltage of 400 kV were carried out. The OCPs were measured by GITT; a constant current of 1.86 mA g^{-1} (= 0.01 C) was applied for 10 h or until the potential reached the cutoff potential (set at 1.0 V), and OCPs were then recorded after the circuit had been in the open-circuit condition for 24 h following the application of current. Transitional potentials were also determined from the GITT traces.

ASSOCIATED CONTENT

Supporting Information

XRD profiles of $CaFeO_3$ after discharge and charge (Figure S1), results of Rietveld analysis of $CaFeO_3$ (Table S1), areas and results of composition analysis of the $CaFeO_z$ particle reduced to n = 0.5 (Figure S2 and Table S2), potential variation during the GITT measurement with OCPs and the average iron valences (Figure S3). This material is available free of charge via the Internet at http://pubs.acs.org.

AUTHOR INFORMATION

Corresponding Authors

tmizuno@mail.ecc.u-tokyo.ac.jp
hibino@appchem.t.u-tokyo.ac.jp

Notes

The authors declare no competing financial interest.

ACKNOWLEDGMENTS

This research was supported by the Japan Society for the Promotion of Science (JSPS) through its "Funding Program for World-Leading Innovative R&D on Science and Technology (FIRST Program)". A part of this work was supported by "Nanotechnology Platform" (Project 12024046) of the Ministry of Education, Culture, Sports, Science and Technology (MEXT), Japan.

REFERENCES

(1) Hu, L.-H.; Wu, F.-Y.; Lin, C.-T.; Khlobystov, A. N.; Li, L.-J. *Nat. Commun.* **2013**, *4*, 1687.
(2) Peng, Z.; Freungerger, S. A.; Chen, Y.; Bruce, P. G. *Science* **2012**, *337*, 563.
(3) Jung, H.-G.; Hassoun, J.; Park, J.-B.; Sun, Y.-K.; Scrosati, B. *Nat. Chem.* **2012**, *4*, 579.
(4) Wei, S. Z.; Li, W.; Cha, J. J.; Zheng, G.; Yang, Y.; McDowell, M. T.; Hsu, P.-C.; Cui, Y. *Nat. Commun.* **2013**, *4*, 1331.
(5) Hayashi, A.; Noi, K.; Sakuda, A.; Tatsumisago, M. *Nat. Commun.* **2012**, *3*, 856.
(6) Yabuuchi, N.; Yoshida, H.; Komaba, S. *Electrochemistry* **2012**, *80*, 716.
(7) Yabuuchi, N.; Kajiyama, M.; Iwatate, J.; Nishikawa, H.; Hitomi, S.; Okuyama, R.; Usui, R.; Yamada, Y.; Komaba, S. *Nat. Mater.* **2012**, *11*, 512.
(8) Lv, D.; Xu, T.; Saha, P.; Datta, M. K.; Gordin, M. L.; Manivannan, A.; Kumta, P. N.; Wang, D. *J. Electrochem. Soc.* **2013**, *160*, A351.
(9) Hibino, M.; Kimura, T.; Suga, Y.; Kudo, T.; Mizuno, N. *Sci. Rep.* **2012**, *2*, 601.
(10) Takano, M.; Nakanishi, N.; Takeda, Y.; Naka, S.; Takada, T. *Mater. Res. Bull.* **1977**, *12*, 923.
(11) Takeda, T.; Kanno, R.; Kawamoto, Y.; Takano, M.; Kawasaki, S.; Kamiyama, T.; Izumi, F. *Solid State Sci.* **2000**, *2*, 673.
(12) Rudolf, P.; Schollhorn, R. *J. Chem. Soc., Chem. Commun.* **1992**, 1158.
(13) Kanamaru, F.; Miyamoto, H.; Mimura, Y.; Koizumi, M.; Shimada, M.; Kume, S. *Mater. Res. Bull.* **1979**, *5*, 257.
(14) Takeda, Y.; Naka, S.; Takano, M.; Shinjo, T.; Takada, T.; Shimada, M. *Mater. Res. Bull.* **1978**, *13*, 61.
(15) As shown in Figure 4, the reduction proceeded in the two-phase system of P- and BM-phases over almost the whole range of the process. The two-phase system in an equilibrium state generally requires a perfect plateau in the potential profile. In the present cathode, not only the P- and BM-phases but also sodium oxides were formed. The increase in the amounts of the sodium oxides would decrease the electronic conductivity of the electrode and increase the overpotential, resulting in the disappearance of the plateau in the two-phase state of the P- and BM-phases in Figure 3.

(16) Nemudry, A.; Rogatchev, A.; Gainutdinov, I.; Schöllhorn, R. *J. Solid State Electrochem.* **2001**, *5*, 450.
(17) The volume increase from $CaFeO_3$ to $CaFeO_{2.5}$ is 5%, which is comparable to those of $LiCoO_2$ (2−3%) and $LiMn_2O_4$ (70% discharge, 5%; full discharge, 8%). However, considering the formation of Na_2O_2 (at n = 0.5) and Na_2O (at n = 1), the volume increases are 26 and 47%, respectively.
(18) IR absorption and Raman scattering spectra showed no band of sodium oxides, and the $Na_2O/CaFeO_{2.5}$ (0.5/1) physical mixture showed no IR and Raman band of Na_2O, suggesting that the amount of Na_2O was lower than detection limit.
(19) Berastegui, P.; Eriksson, S.-G.; Hull, S. *Mater. Res. Bull.* **1999**, *34*, 303.
(20) Föppel, H. *Z. Anorg. Allg. Chem.* **1957**, *291*, 12.
(21) Chase, M. W., Jr. *NIST-JANAF Thermochemical Tables*, 4th ed.; Journal of Physical and Chemical Reference Data Monograph *9*; 1998.